PAPER

Theoretical investigation of the ORR on boron–silicon nanotubes (B–SiNTs) as acceptable catalysts in fuel cells

Razieh Razavi *[a] and Meysam Najafi [ORCID] *[b]

Here, the potential of boron doped silicon nanotubes (7, 0) as ORR catalysts is examined. Acceptable paths for the ORR on studied catalysts are examined through DFT. The optimum mechanism of the ORR on the surface of B_2–SiNT (7, 0) is shown. The ORR on the surface of B_2–SiNTs (7, 0) can continue through LH and ER mechanisms. The calculated beginning voltage for the ORR on B_2–SiNTs (7, 0) is 0.37 V and it is smaller than the beginning voltage (0.45 V) for platinum-based catalysts. In the acidic solution the beginning voltage for the oxygen reduction process can be evaluated to be 0.97 V, which corresponds to 0.37 V as a minimum overvoltage for the ORR. The B_2–SiNTs (7, 0) are suggested as an ORR catalyst in acidic environments.

1. Introduction

Fuel cells as energy machines are important due to their low contamination and great efficiency. The ORR rate in electrodes of cells is slow, therefore the ORR can be evaluated as a significant reason to increase the full cell efficiency.[1–4] Platinum-compounds have been used as catalysis in the ORR but platinum-compounds have low ability to endure CO.[5–9]

The potential of various compounds was investigated to find and propose effective catalysts for the ORR. Nanostructures and doped nanostructures with high ability for CO endurance can be used as suitable replacements for platinum-compounds.[10–15] The B-nanostructures are acceptable catalysts for the ORR in alkaline conditions and mechanisms of action of B-doped nanostructures in acidic position are not clear.[16–23]

The nanostructures due to their electrical conductivity and thermal conductivity can be used to product the transistors and non-volatile memory devices.[24–28] The electrical conductivity of doped carbon/silicon nanotubes indicated that the adoption of carbon/silicon nanotubes (with various atoms such as B, N, O and some metals) increased their electrical conductivity, significantly. These findings improved the application of carbon/silicon nanotubes in nano-electronic devices and novel catalyst to ORR.[29–38] Results demonstrated that the adoption of carbon/silicon nanotubes increased their electrical conductivity and enhanced the ORR efficiency.[39–48]

Wang *et al.*[49] demonstrated that boron-doped graphene nanoribbons are suitable catalyst to ORR catalyst. Xiao *et al.*[50] proved

that the layered silicon–carbon nano sheets represented the high activity in ORR without CO poisoning. Xia and Zhang *et al.*[51,52] investigated the mechanisms of ORR of fuel cells in acidic environment on graphene cathodes. Stevenson *et al.*[53] proved in ORR the O_2 in a 2-electron path is reduced to form OOH on carbon nanotubes. Hu and Xiong *et al.*[54,55] confirmed that nitrogen and boron-doped nanostructures as ORR catalysts have low price, great durability and excellent potential. Zhao and Wei *et al.*[56,57] confirmed the doping of carbon nanotubes have vital roles on performance of ORR. Ferrighi *et al.*[58] demonstrated that boron atoms of nanosheets increase the reactions of oxygen with graphene.

In current study, ORR on B-doped silicon nanotube (7, 0) as acceptable catalysts is examined to find possible mechanisms to ORR on B_2–SiNT (7, 0) and to suggest high activity nanocatalysts to ORR.

2. Computational details

In this study the silicon nanotube (length and diameter are 1 and 0.475 nm) is modeled and their open elements are saturated with hydrogen atoms to elude border effects. The geometries of nanotubes and studied molecules (such as OOH, OH, H_2O and CO) are optimized by M06-2X/6-311G+ (2d, 2p) in GAMESS package.[59–72] The consistent field is investigated by 10^{-6} Hartree as convergence value. Vibrational frequencies of nanotubes and molecules by M06-2X/6-311G+ (2d, 2p) are calculated.

In the density functional, M06 functionals are extremely parameterized proximate exchange functionals theory and they are supported on generalized gradient approximation (meta-GGA). These functionals are used for traditional quantum chemistry, solid-state physics calculations and thermodynamic values of reactions.[73–82] M06-2X as the most accurate functional

[a] Department of Chemistry, Faculty of Science, University of Jiroft, Jiroft, Iran. E-mail: R.Razavi@ujiroft.ac.ir

[b] Medical Biology Research Center, Health Technology Institute, Kermanshah University of Medical Sciences, Kermanshah, Iran. E-mail: iau.mnajafi@yahoo.com

of Minnesota functional is a Global hybrid functional with 54% HF exchange and it is the ascendancy constructor within the 06 functionals for thermochemistry, kinetics and various chemical interactions.[73–82] The M06-2X functional as hybrid meta exchange–correlation functionals present 32 empirically improved factors within the exchange–correlation functional.[83–87]

The energy and Gibbs free energy ($G = E_0 + ZPE + \Delta H + RT - TS$) values of nanotubes are calculated. The E_0 and ZPE are electronic energy and zero-point energy and T is 298.15 K.[59–72] Adoption energy (E_{doped}) and Gibbs free energy adoption (G_{doped}) of B atoms in SiNT (7, 0) are calculated:

$$E_{doped} = E(\text{B–SiNT}) - E(\text{SiNT}) - E(\text{B}) \quad (1)$$

$$G_{doped} = G(\text{B–SiNT}) - G(\text{SiNT}) - G(\text{B}) \quad (2)$$

$$E_{doped} = E(\text{B}_2\text{–SiNT}) - E(\text{SiNT}) - 2E(\text{B}) \quad (3)$$

$$G_{doped} = G(\text{B}_2\text{–SiNT}) - G(\text{SiNT}) - 2G(\text{B}) \quad (4)$$

$E(\text{B–SiNT (7, 0)})$ and $E(\text{B}_2\text{–SiNT (7, 0)})$ are energies of B–SiNT (7, 0) and B_2–SiNT (7, 0).

Energy adsorption (ΔE_{ad}) and Gibbs free energy adsorption (ΔG_{ad}) of molecules (such as OOH, OH, H_2O and CO) on surfaces of studied nanotubes (SiNT, B–SiNT, B–B–SiNT and B_2–SiNT) are calculated:

$$\Delta E_{ad} = E(\text{molecule–nanotube}) - E(\text{nanotube}) - E(\text{molecule}) \quad (5)$$

$$\Delta G_{ad} = G(\text{molecule–nanotube}) - G(\text{nanotube}) - G(\text{molecule}) \quad (6)$$

$E(\text{molecule–nanotube})$ and $G(\text{molecule–nanotube})$ are E and G of molecules–nanotubes. $G(\text{nanotube})$ and $G(\text{molecule})$ are G of nanotubes and molecules. $E(\text{nanotube})$ and $G(\text{molecule})$ are energy and G of nanotubes and molecules. Natural bond orbital charges (q) and gap energy (E_{HLG}) complexes are calculated[59–72] and transition state, reaction energy (ΔE_r) and activation barrier energy (ΔE_a) are examined by LST/QST method and M06-2X.[64]

Activation energy ($\Delta E_a = E_{TS} - E_{IS}$) is difference of energy between transition (E_{TS}) and initial (E_{IS}) studied complexes. In this study, the reaction energy ($\Delta E_a = E_{FS} - E_{IS}$) is difference of energy between final (E_{FS}) and initial (E_{IS}) studied complexes.[88–95] The ΔG of ORR on B_2–SiNT (7, 0) in according to standard hydrogen electrode was evaluated through $\Delta G = \Delta E + \Delta ZPE - T\Delta S + \Delta G_U + \Delta G_{pH}$ (obtained data were reported in Fig. 5).[96–104] ΔG_{pH} ($\Delta G_{pH} = kT \ln 10 \times pH$) is modification of proton Gibbs free energy and $\Delta G_U = -neU$. The n, e and U are electrons, first charge and electrode potential. The U is requested potential and overvoltage is $\eta = U_0 - U$.[49–58] Conductor like screening method is used to estimate water environment (dielectric constant is 78.54).[59–72]

3. Results and discussion

3.1. Molecule adsorptions on nanotube

In this section, the B adoption of SiNT (7, 0) were investigated and then interactions of B–SiNT (7, 0) structures with O_2, OOH,

OH, H_2O and CO molecules were investigated. The one Si atom of the SiNT (7, 0) was replaced with one B atom and the B–SiNT (7, 0) was produced (Fig. 1). Also the two Si atoms of the SiNT (7, 0) in two difference positions were replaced with two B atoms and B–B–SiNT (7, 0) and B_2–SiNT (7, 0) structures were produced (Fig. 1). Structures of SiNT, B–SiNT, B–B–SiNT, B_2–SiNT, O_2, OH, H_2O, H_2O_2 and CO are presented in Fig. 1. The adoption energy (E_{doped}), adoption free Gibbs energy (G_{doped}) and bond lengths of B–Si of B–SiNT (7, 0), B–B–SiNT (7, 0) and B_2–SiNT (7, 0) were reported in Fig. 1. In the B–SiNT (7, 0) the B atom was connected with three neighboring silicon atoms and the E_{doped} and G_{doped} were −2.18 and −2.10 eV and average of bonds of B–Si in B–SiNT (7, 0) is 1.95 Å. In the B–B–SiNT (7, 0) the B atoms are connected with four neighboring silicon atoms and the E_{doped} and G_{doped} are −2.23 and −2.14 eV and average of bonds of B–Si in B–B–SiNT (7, 0) is 1.93 Å. In the B_2–SiNT (7, 0) the B atoms are connected with six neighboring silicon atoms and the E_{doped} and G_{doped} values are −2.28 and −2.17 eV and average of bonds of B–Si in B_2–SiNT (7, 0) are 1.92 Å.

The q and E_{HLG} of SiNT (7, 0), B–SiNT (7, 0), B–B–SiNT (7, 0) and B_2–SiNT (7, 0) are stated in Table 1. E_{HLG} of SiNT (7, 0), B–SiNT (7, 0), B–B–SiNT (7, 0) and B_2–SiNT (7, 0) are 1.84, 1.75, 1.68 and 1.64 eV. The q of B–SiNT (7, 0), B–B–SiNT (7, 0) and B_2–SiNT (7, 0) are 0.58, 0.69 and 0.73|e|. The |E_{doped}|, |G_{doped}| and q values of B_2–SiNT (7, 0) are higher than B–SiNT (7, 0) and B–B–SiNT (7, 0). Results showed that the E_{HLG} value of B_2–SiNT (7, 0) is lower than corresponding values on surfaces of B–SiNT (7, 0) and B–B–SiNT (7, 0). Therefore, it can be concluded that the B_2–SiNT (7, 0) is the most stable than B–SiNT (7, 0) and B–B–SiNT (7, 0) from thermodynamic view point. The B atoms in B–SiNT (7, 0), B–B–SiNT (7, 0) and B_2–SiNT (7, 0) structures are advantageous to adsorption of O_2 molecule and these B atoms are active positions of B–SiNT (7, 0), B–B–SiNT (7, 0) and B_2–SiNT (7, 0) as catalyst for ORR. Therefore, B atoms are essential location to adsorption of O_2 molecule and B atoms can be considered as initiator of first ORR step.

Therefore, O_2 adsorption on SiNT (7, 0), B–SiNT (7, 0), B–B–SiNT (7, 0) and B_2–SiNT (7, 0) were investigated. The possible positions of SiNT (7, 0), B–SiNT (7, 0), B–B–SiNT (7, 0) and B_2–SiNT (7, 0) to O_2 adsorption including top position B atom and bridge positions of B–Si, B–B and Si–Si bonds were examined in Fig. 2. The B–O, O–O and Si–O in SiNT (7, 0), B–SiNT (7, 0), B–B–SiNT (7, 0) and B_2–SiNT (7, 0) with O_2 are presented in Fig. 2 (2a–2l structures). The ΔE_{ad} and ΔG_{ad} of O_2 on SiNT (7, 0), B–SiNT (7, 0), B–B–SiNT (7, 0) and B_2–SiNT (7, 0) are displayed in Table 2. |ΔG_{ad}| of O_2 on B–SiNT, B–B–SiNT and B_2–SiNT are greater than SiNT (7, 0). The |ΔE_{ad}| and |ΔG_{ad}| of O_2 on B_2–SiNT (7, 0) are greater than B–SiNT (7, 0), B–B–SiNT (7, 0). The bridge position of B–B in B_2–SiNT (7, 0) is stable than top position B in B_2–SiNT (7, 0) to O_2 adsorption.

Wang, Xiao and Xia et al.[49–51] calculated the O_2 adsorption on surfaces of boron-doped graphene nanoribbon, silicon–carbon nano sheets and B and N doped-graphene by theoretical methods, respectively (results reported in Table 4). The ΔE_{ad} of O_2 on B-doped graphene, silicon–carbon nano-sheets and N-doped graphene are −0.62, −0.53 and −0.60 eV. Therefore ΔE_{ad} value (−0.61 eV) of O_2 on B_2–SiNT (7, 0) in present study is
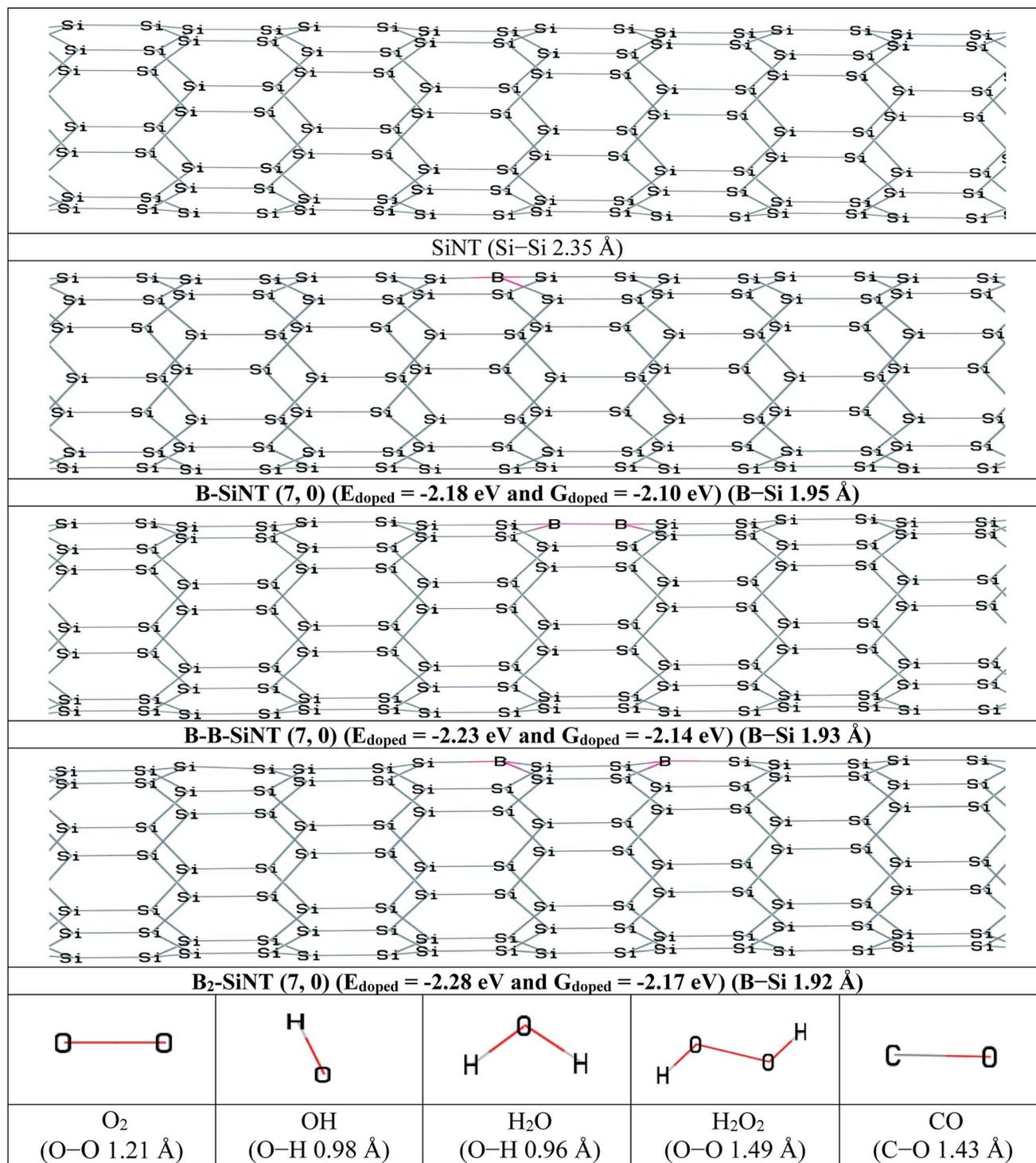
Fig. 1 The initial structures of SiNT, B–SiNT, B–B–SiNT and B$_2$–SiNT and O$_2$, OH, H$_2$O, H$_2$O$_2$ and CO molecules.

similar to corresponding values of O$_2$ on various nanostructures were calculated in previous theoretical works.[49–51]

The charge transfer (q) and HOMO–LUMO band gap (E_{HLG}) of the complexes of SiNT (7, 0), B–SiNT (7, 0), B–B–SiNT (7, 0) and B$_2$–SiNT (7, 0) with O$_2$ molecule are displayed in Table 1. The E_{HLG} values of O$_2$ adsorption on B–SiNT (7, 0), B–B–SiNT (7,

0) and B$_2$–SiNT (7, 0) are lower than SiNT (7, 0). The E_{HLG} values of O$_2$ adsorption on B$_2$–SiNT (7, 0) are lower than B–SiNT (7, 0), B–B–SiNT (7, 0). The bridge position of B–B in B$_2$–SiNT (7, 0) has higher q and lower E_{HLG} than top position B in B$_2$–SiNT (7, 0) to O$_2$ adsorption. Complex of B$_2$–SiNT (7, 0) with O$_2$ molecule (**2d** structure) is the most stable than other complexes of B–SiNT (7,

Table 1 Charge transfer (q) (in $|e|$) and HOMO–LUMO band gap (E_{HLG}) (in eV) of studied complexes

Complex	q	E_{HLG}	Complex	q	E_{HLG}	Complex	q	E_{HLG}	Complex	q	E_{HLG}
SiNT	—-	1.84	*B–SiNT*	0.58	1.75	*B–B–SiNT*	0.69	1.68	*B₂–SiNT*	0.73	1.64
2a	0.36	1.69	*2b*	0.47	1.61	*2c*	0.59	1.52	*2d*	0.64	1.48
2e	0.29	1.75	*2f*	0.39	1.68	*2g*	0.51	1.59	*2h*	0.58	1.55
2i	0.32	1.72	*2j*	0.43	1.64	*2k*	0.54	1.56	*2l*	0.61	1.52
2m	0.49	1.35	*2n*	0.62	1.23	*2o*	0.73	1.17	*2p*	0.82	1.14
3a	0.41	1.54	*3b*	0.51	1.45	*3c*	0.65	1.38	*3d*	0.73	1.25
3e	0.59	1.14	*3f*	0.81	1.05	*3g*	0.84	0.99	*3h*	0.91	0.95
3m	0.11	1.80	*3n*	0.14	1.70	*3o*	0.19	1.62	*3p*	0.21	1.60
3q	0.08	1.82	*3r*	0.12	1.72	*3s*	0.15	1.64	*3t*	0.18	1.63

0) and B–B–SiNT (7, 0) with O₂ molecule from thermodynamic view point. It can be concluded that O₂ adsorbed on B₂–SiNT (7, 0) in figure *2d* significantly and there are suitable interactions between the O₂ molecule and B₂–SiNT (7, 0) and the adsorption of O₂ molecules on studied surfaces are chemical adsorption processes.
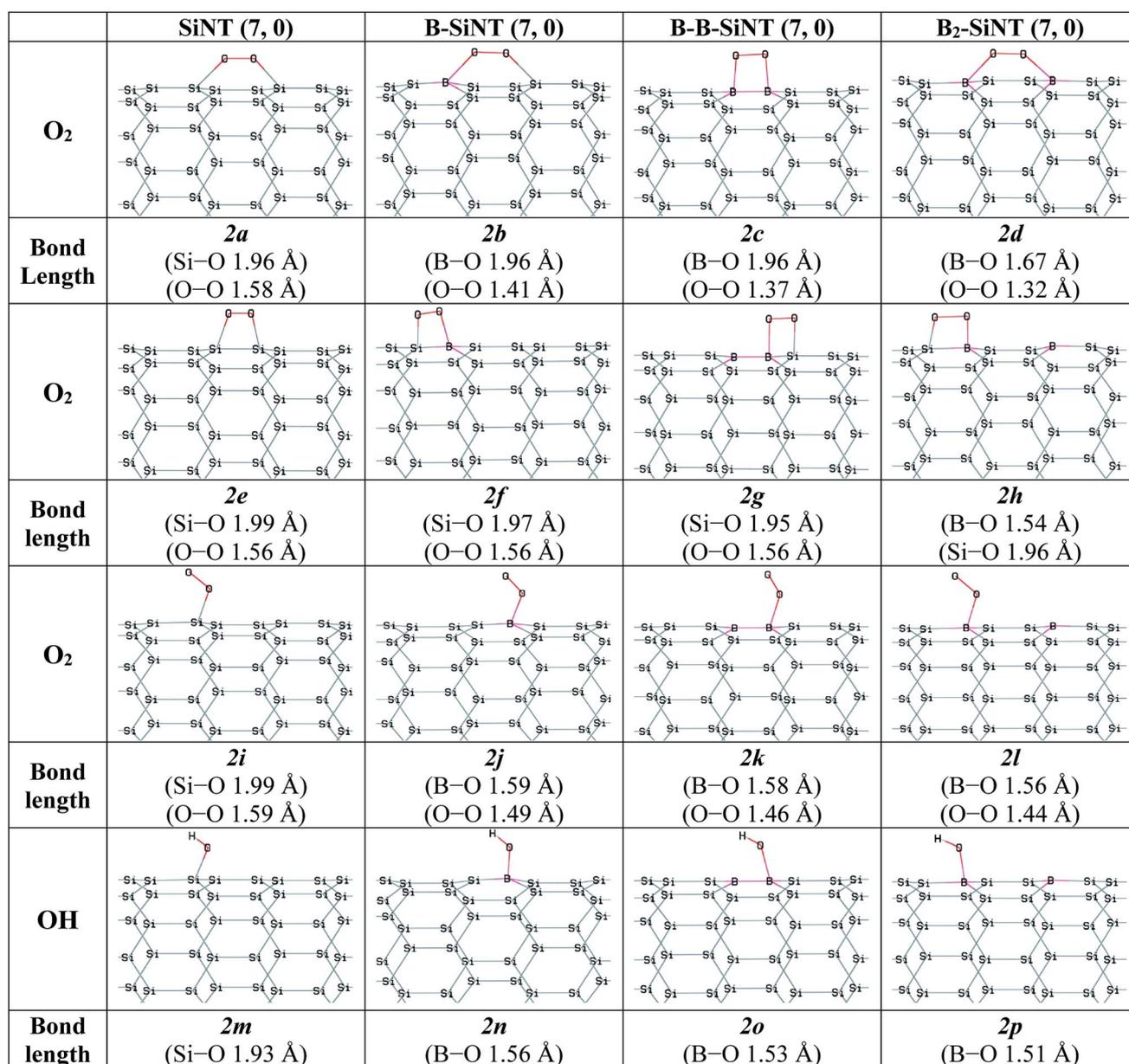

Fig. 2 Complexes of the SiNT (7, 0), B–SiNT (7, 0), B–B–SiNT (7, 0) and B₂–SiNT (7, 0) with O₂ and OH molecules.

Table 2 The ΔE_{ad} (in eV) and ΔG_{ad} (in eV) values of studied complexes

Complex	ΔE_{ad}	ΔG_{ad}	Complex	ΔE_{ad}	ΔG_{ad}	Complex	ΔE_{ad}	ΔG_{ad}	Complex	ΔE_{ad}	ΔG_{ad}
2a	−0.41	−0.36	*2b*	−0.61	−0.54	*2c*	−0.84	−0.79	*2d*	−0.88	−0.81
2e	−0.39	−0.33	*2f*	−0.42	−0.38	*2g*	−0.55	−0.51	*2h*	−0.61	−0.55
2i	−0.27	−0.24	*2j*	−0.64	−0.61	*2k*	−0.69	−0.64	*2l*	−0.73	−0.68
2m	−2.07	−1.97	*2n*	−2.23	−2.15	*2o*	−2.31	−2.21	*2p*	−2.39	−2.28
3a	−0.87	−0.81	*3b*	−1.06	−0.99	*3c*	−1.11	−1.03	*3d*	−1.17	−1.12
3e	−3.11	−2.97	*3f*	−3.59	−3.45	*3g*	−3.67	−3.56	*3h*	−3.79	−3.67
3i	−2.24	−2.13	*3j*	−2.25	−2.15	*3k*	−2.27	−2.17	*3l*	−2.31	−2.21
3m	−0.15	−0.10	*3n*	−0.18	−0.13	*3o*	−0.20	−0.15	*3p*	−0.24	−0.19
3q	−0.09	−0.05	*3r*	−0.10	−0.07	*3s*	−0.11	−0.08	*3t*	−0.14	−0.12

In this study the interactions of important intermediates such as O, H, OOH, OH, H_2O and CO molecules with SiNT (7, 0), B–SiNT (7, 0), B–B–SiNT (7, 0) and B_2–SiNT (7, 0) surfaces in process of ORR were investigated (Fig. 2 and 3). The bonds of Si–O of SiNT (7, 0), B–SiNT (7, 0), B–B–SiNT (7, 0) and B_2–SiNT (7, 0) with molecules are stated. E_{HLG}, q, ΔE_{ad}, ΔG_{ad} of molecules on SiNT (7, 0), B–SiNT (7, 0), B–B–SiNT (7, 0) and B_2–SiNT (7, 0) are reported in Tables 1 and 2. OOH and OH intermediates can be adsorb on B site of B–SiNT (7, 0), B–B–SiNT (7, 0) and B_2–SiNT (7, 0). The O intermediate has tendency to adsorb on B–Si and B–B bridge positions of B–SiNT (7, 0), B–B–SiNT (7, 0) and B_2–SiNT (7, 0). It can be concluded that the complexes of B_2–SiNT (7, 0) with O, H, OOH, OH and H_2O molecules are stable than SiNT (7, 0), B–SiNT (7, 0) and B–B–SiNT (7, 0).

Wang, Xiao and Xia et al.[49–51] calculated the O, OH and OOH adsorption on surfaces of boron-doped graphene nanoribbon, silicon–carbon nano sheets and B and N doped-graphene by theoretical methods, respectively (results reported in Table 4). ΔE_{ad} of O on B-doped graphene, silicon–carbon nano-sheets and N-doped graphene were −3.74, −4.11 and −3.55 eV. ΔE_{ad} of OH on boron-doped graphene, silicon–carbon nano-sheets and N-doped graphene were −2.38, −2.87 and −2.41 eV. ΔE_{ad} of OOH on B-doped graphene, silicon–carbon nano-sheets and N-doped graphene are −1.12, −1.18 and −1.06 eV. ΔE_{ad} values of O, OH and OOH (−1.17, −2.39 and −1.17 eV) on B_2–SiNT (7, 0) in present study are similar to corresponding values of O, OH and OOH on various nano-structures were calculated in previous theoretical works.[49–51]

The H_2O molecule favored to adsorb on above ring position of SiNT (7, 0), B–SiNT (7, 0), B–B–SiNT (7, 0) and B_2–SiNT (7, 0)

and the average of ΔE_{ad} and ΔG_{ad} values are −0.19 and −0.14 eV. The average of q and E_{HLG} values for adsorption of H_2O molecule on SiNT (7, 0), B–SiNT (7, 0), B–B–SiNT (7, 0) and B_2–SiNT (7, 0) surface is 0.16|e| and 1.68 eV. H_2O molecule can be adsorbed on SiNT (7, 0), B–SiNT (7, 0), B–B–SiNT (7, 0) and B_2–SiNT (7, 0) surfaces as physical adsorption processes.

In process of ORR the CO can occupy the positions of catalysts and the performance of ORR is reduced and efficiency of catalyst decreases sharply. Previous works showed that reactions between CO molecule and surface of platinum nano-catalyst was powerful (ΔE_{ad} is −1.90 eV) and CO poisoning was happen.[20,66] The average of ΔE_{ad} and ΔG_{ad} of CO on SiNT, B–SiNT, B–B–SiNT and B_2–SiNT surfaces are −0.11 and −0.08 eV. The average of q and E_{HLG} values for adsorption of CO on SiNT (7, 0), B–SiNT (7, 0), B–B–SiNT (7, 0) and B_2–SiNT (7, 0) surface is 0.13|e| and 1.70 eV. The CO molecule can be adsorbed on SiNT (7, 0), B–SiNT (7, 0), B–B–SiNT (7, 0) and B_2–SiNT (7, 0) surfaces as physical adsorption processes. It can be concluded that B_2–SiNT (7, 0) as acceptable catalyst can be endurance to CO poisoning and it can solve the major problem of platinum nano-catalysts.

Wang, Xiao and Xia et al.[49–51] calculated the H_2O and CO adsorption on surfaces of boron-doped graphene nanoribbon, silicon–carbon nano sheets and B and N doped-graphene. The ΔE_{ad} of H_2O on surfaces of B-doped graphene, silicon–carbon nano-sheets and N-doped graphene were −0.24, −0.18 and −0.08 eV. The ΔE_{ad} of CO on surfaces of B-doped graphene, silicon–carbon nano-sheets and N-doped graphene were −0.17, −0.07 and −0.12 eV. The ΔE_{ad} of H_2O and CO (−0.24 and −0.14 eV) on B_2–SiNT (7, 0) in present study are similar to

Table 3 The ΔE_a and ΔE_r for ORR on B_2–SiNT (7, 0)

Path	Studied reaction steps	ΔE_a (eV)	ΔE_r (eV)
1	O_2 + B_2–SiNT (7, 0) → B_2–SiNT (7, 0)–*O_2	—	−0.68
1	B_2–SiNT (7, 0)–*O_2 + H^+ + e^- → B_2–SiNT (7, 0)–*OOH	0.00	−1.07
1	B_2–SiNT (7, 0)–*OOH + H^+ + e^- → B_2–SiNT (7, 0)–*O + H_2O	0.18	−2.75
1	B_2–SiNT (7, 0)–*O + H^+ + e^- → B_2–SiNT (7, 0)–*OH	0.37	−1.57
1	B_2–SiNT (7, 0)–*OH + H^+ + e^- → B_2–SiNT (7, 0)* + H_2O	0.07	−1.34
2	O_2 + B_2–SiNT (7, 0) → B_2–SiNT (7, 0)–*O_2	—	−0.68
2	B_2–SiNT (7, 0)–*O_2 + H^+ + e^- → B_2–SiNT (7, 0)–*OOH	0.00	−1.07
2	B_2–SiNT (7, 0)–*OOH + H^+ + e^- → *OH–B_2–SiNT (7, 0)–*OH	0.24	−2.97
2	*OH–B_2–SiNT (7, 0)–*OH + H^+ + e^- → B_2–SiNT (7, 0)–*OH + H_2O	0.35	−1.20
2	B_2–SiNT (7, 0)–*OH + H^+ + e^- → B_2–SiNT (7, 0)* + H_2O	0.07	−1.34

	SiNT (7, 0)	B–SiNT (7, 0)	B–B–SiNT (7, 0)	B₂–SiNT (7, 0)
OOH				
Bond length	3a (Si–O 1.95 Å) (O–O 1.54 Å)	3b (B–O 1.51 Å) (O–O 1.51 Å)	3c (B–O 1.49 Å) (O–O 1.49 Å)	3d (B–O 1.53 Å) (O–O 1.47 Å)
O				
Bond length	3e (Si–O 1.85 Å)	3f (Si–O 1.83 Å) (B–O 1.47 Å)	3g (B–O 1.45 Å)	3h (Si–O 1.81 Å) (B–O 1.43 Å)
H				
Bond length	3i (Si–H 1.66 Å)	3j (Si–H 1.64 Å)	3k (Si–H 1.63 Å)	3l (Si–H 1.64 Å)
H₂O				
Distance	3m (distance 3.21 Å)	3n (distance 3.17 Å)	3o (distance 3.14 Å)	3p (distance 3.11 Å)
CO				
Distance	3q (distance 3.34 Å)	3r (3.27 Å)	3s (distance 3.25 Å)	3t (distance 3.22 Å)

Fig. 3 Complexes of the SiNT (7, 0), B–SiNT (7, 0), B–B–SiNT (7, 0) and B₂–SiNT (7, 0) with O and H atoms, OOH, H₂O and CO molecules.

corresponding values of H_2O and CO on various nanostructures were calculated in previous theoretical works.[49–51]

3.2. B₂–SiNT (7, 0) as catalyst to ORR

Nano-catalysts processed the chemical reactions through the ER and LH paths. The paths for ORR via B₂–SiNT (7, 0) as acceptable catalyst through the LH and ER mechanisms were investigated. As start, O_2 adsorption is investigated via O_2 dissociation or hydrogenation of O_2 to create B₂–SiNT (7, 0)–*OOH. Firstly, the O_2 dissociation process can be defined as B₂–SiNT (7, 0)–*O_2 → *O–B₂–SiNT (7, 0)–*O. The dissociated O atoms were elected to link on B–Si position and activation barrier energy is 0.96 eV (figures 2a (IS), 2b (TS) and 2c (FS)).
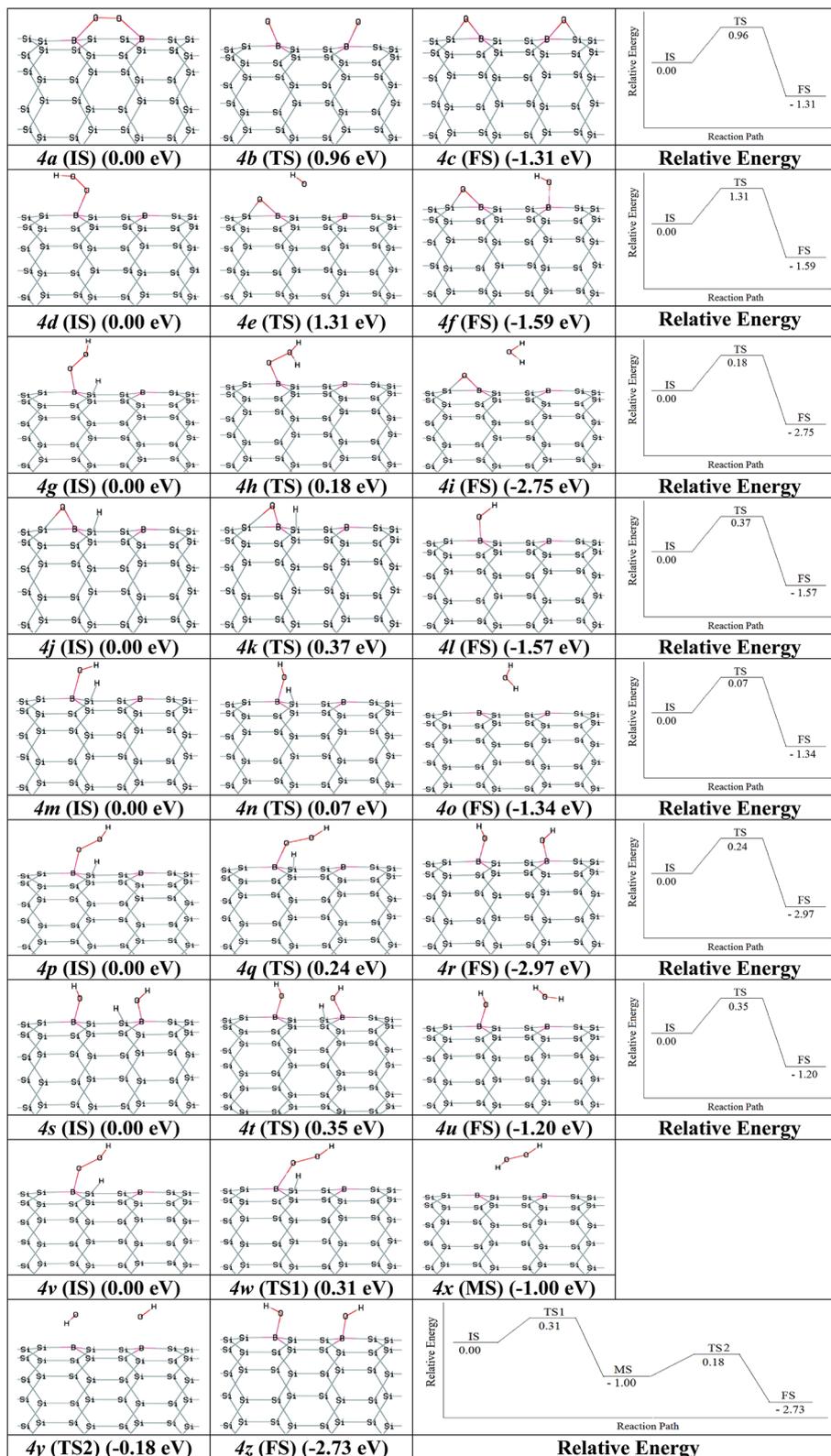
Fig. 4 The intermediates of ORR and relative energies: (1) B_2–SiNT (7, 0)–$*O_2$ → $*O$–B_2–SiNT (7, 0)–$*O$; (2) B_2–SiNT (7, 0)–$*OOH$ → $*O$–B_2–SiNT (7, 0)–$*OH$; (3) B_2–SiNT (7, 0)–$*OOH$ → B_2–SiNT (7, 0)–$*O$ + H_2O; (4) B_2–SiNT (7, 0)–$*O$ → B_2–SiNT (7, 0)–$*OH$; (5) B_2–SiNT (7, 0)–$*OH$ → B_2–SiNT (7, 0)–$*$ + H_2O; (6) B_2–SiNT (7, 0)–$*OOH$ → $*OH$–B_2–SiNT (7, 0)–$*OH$; (7) $*OH$–B_2–SiNT (7, 0)–$*OH$ → $*OH$–B_2–SiNT (7, 0) + H_2O; (8) B_2–SiNT (7, 0)–$*OOH$ → B_2–SiNT (7, 0) + H_2O_2 →$*OH$–B_2–SiNT (7, 0)–$*OH$.

Table 4 The ΔE_{ad} (in eV) values of O$_2$, O, OH and OOH on B-doped graphene, silicon−carbon nano-sheets and N-doped graphene[65–67] and B−SiNT (7, 0), B−B−SiNT (7, 0) and B$_2$−SiNT (7, 0) in this study
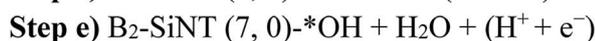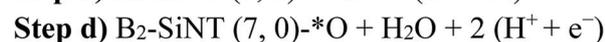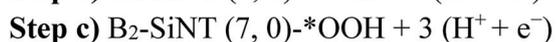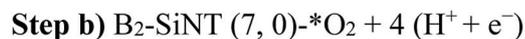
Catalysts/species	B-doped graphene[49]	Si−C nano-sheet[50]	N-doped graphene[51]	B−SiNT (7, 0)	B−B−SiNT (7, 0)	B$_2$−SiNT (7, 0)
O$_2$	−0.62	−0.53	−0.60	−0.69	−0.84	−0.88
O	−3.74	−4.11	−3.55	−3.59	−3.67	−3.79
OH	−2.38	−2.87	−2.41	−2.23	−2.31	−2.39
OOH	−1.12	−1.18	−1.06	−1.06	−1.11	−1.17

Secondary, adsorbed O$_2$ can interact *via* H atom to create B$_2$−SiNT (7, 0)−*OOH as follow: B$_2$−SiNT (7, 0)−*O$_2$ + H$^+$ + e$^-$ → B$_2$−SiNT (7, 0)−*OOH, this process has no any activation barrier energy.

The OOH adsorption on of B$_2$−SiNT (7, 0) has higher ΔE_{ad} than O$_2$ *ca.* 0.29 eV and also O$_2$ dissociation on surface of B$_2$−SiNT (7, 0) has high activation barrier energy. H atom is added into Si in B$_2$−SiNT (7, 0)−*OOH and H atom reacted *via* B$_2$−SiNT

(7, 0)−*OOH. Then the B$_2$−SiNT (7, 0)−*OOH dissociated to *O−B$_2$−SiNT (7, 0)−*OH (figures *2d* (IS), *2e* (TS) and *2f* (FS)), due to great activation barrier energy (1.31 eV) this process is impossible. The creation of B$_2$−SiNT (7, 0)−*OOH in ORR on B$_2$−SiNT (7, 0) is suitable than dissociation of O$_2$ molecule.

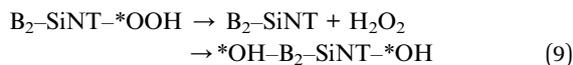The ORR is done through the B$_2$−SiNT−*OOH intermediate as follows:

Step a) B$_2$-SiNT (7, 0)* + O$_2$ + 4 (H$^+$ + e$^-$)   **Step b)** B$_2$-SiNT (7, 0)-*O$_2$ + 4 (H$^+$ + e$^-$)
Step c) B$_2$-SiNT (7, 0)-*OOH + 3 (H$^+$ + e$^-$)   **Step d)** B$_2$-SiNT (7, 0)-*O + H$_2$O + 2 (H$^+$ + e$^-$)
Step e) B$_2$-SiNT (7, 0)-*OH + H$_2$O + (H$^+$ + e$^-$)   **Step f)** B$_2$-SiNT (7, 0)*+ 2 H$_2$O
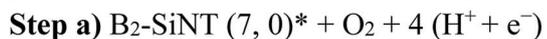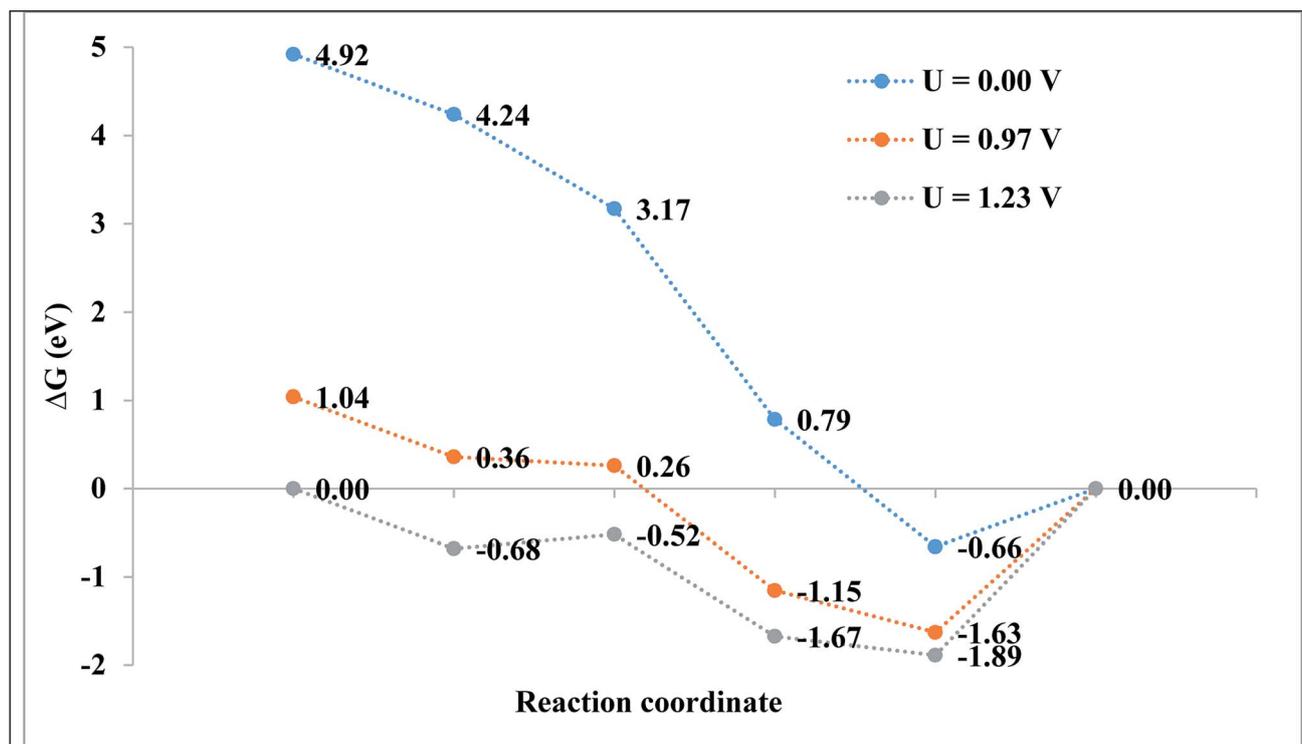
Step	U = 0.00 V	U = 0.97 V	U = 1.23 V	Step	U = 0.00 V	U = 0.97 V	U = 1.23 V
a	4.92	1.04	0.00	d	0.79	-1.15	-1.67
b	4.24	0.36	-0.68	e	-0.66	-1.63	-1.89
c	3.17	0.26	-0.52	f	0.00	0.00	0.00

Fig. 5 The G values for ORR on B$_2$−SiNT (7, 0).

Table 5 The onset-potential (in eV) values for the ORR performed on several catalysts[105–110]

Catalyst	Onset potential	Catalyst	Onset potential	Catalyst	Onset potential
Pd/CNT[105]	0.764	Pd–Ni[107]	1.105	PdNi[109]	1.040
Pd/MWCNT[105]	1.014	PtCo/C[107]	0.836	Pd[109]	0.901
Pd–Ni(3 : 1)/C[106]	1.005	Pd–Fe/C[108]	0.865	Pd–Cu[110]	1.001
Pd$_2$Co/C[106]	0.735	Pd/C[108]	0.920	Pt/C[110]	0.900

$$B_2\text{–SiNT–}^*OOH \rightarrow B_2\text{–SiNT–}^*O + H_2O \quad (7)$$

$$B_2\text{–SiNT–}^*OOH \rightarrow {}^*OH\text{–}B_2\text{–SiNT–}^*OH \quad (8)$$

$$B_2\text{–SiNT–}^*OOH \rightarrow B_2\text{–SiNT} + H_2O_2$$
$$\rightarrow {}^*OH\text{–}B_2\text{–SiNT–}^*OH \quad (9)$$

In path 1, B$_2$–SiNT (7, 0)–*OOH intermediate was decreased to H$_2$O molecule and B$_2$–SiNT (7, 0)–*O ($\Delta E_a = 0.18$ eV). In this process, O–O is fragmented and the first H$_2$O molecule is created (figures *2g* (IS), *2h* (TS) and *2i* (FS)). Then two hydrogenation stages were done and B$_2$–SiNT (7, 0)–*OH (figures *2j* (IS), *2k* (TS) and *2l* (FS)) and the second H$_2$O molecule was created (figures *2m* (IS), *2n* (TS) and *2o* (FS)). The activation barrier energies of these two hydrogenation processes are 0.37 and 0.07 eV, respectively.

In path 2, H atom is linked to O and *OH–B$_2$–SiNT (7, 0)–*OH is created and activation barrier energy is 0.24 eV (figures *2p* (IS), *2q* (TS) and *2r* (FS)). Then, *OH–B$_2$–SiNT (7, 0)–*OH linked to H atom and the first H$_2$O molecule is created and activation barrier energy of this stage is 0.35 eV (figures *2s* (IS), *2t* (TS) and *2u* (FS)). In the end stage of path 2, the B$_2$–SiNT (7, 0)–*OH is hydrogenated and in this step the second H$_2$O molecule is separated.

In the path 3, the B$_2$–SiNT (7, 0)–*OOH is hydrogenated and the H$_2$O$_2$ molecule and B$_2$–SiNT (7, 0) catalyst are created and activation barrier is 0.31 eV (figures *2v* (IS), *2w* (TS1), *2x* (MS), *2y* (TS2) and *2z* (FS)). The H$_2$O$_2$ molecule creation is a mediated state (MS) on surface of B$_2$–SiNT (7, 0) and it cannot effect on potential of the B$_2$–SiNT (7, 0), significantly. In next stage of path 3, separated H$_2$O$_2$ dissociated into *OH–B$_2$–SiNT (7, 0)–*OH structure and therefore H$_2$O$_2$ dissociation has activation barrier energy about 0.82 eV. The ORR *via* path 3 continued *via* two hydrogenation stage as presented in path 1 in Fig. 4 (figures *4s* (IS), *4t* (TS) and *4u* (FS)) and path 2 in Fig. 4 (figures *4m* (IS), *4n* (TS) and *4o* (FS)).

The parameters of two acceptable paths about reduction of B$_2$–SiNT (7, 0)–*OOH structure are stated in Table 3. In path 1, rate-determining stage ($\Delta E_a = 0.37$ eV) on B$_2$–SiNT (7, 0) surface is creation of B$_2$–SiNT (7, 0)–*OH. In path 2, creation of B$_2$–SiNT (7, 0)–*OH structure and H$_2$O molecule is rate-determining stage ($\Delta E_a = 0.35$ eV). In path 2, creation of *OH–B$_2$–SiNT (7, 0)–*OH has higher ΔE_a than formation of B$_2$–SiNT (7, 0)–*O + H$_2$O in path 1 *ca.* 0.06 eV and so path 1 can be considered as optimal pathway to ORR.

The over-potential of ORR on Pt-based compounds and graphene are 0.44 and 0.45 V.[49–59] The experimental researchers investigated the onset-potential for the ORR performed on several catalysts[105–110] and results are stated in Table 5. The G of ORR steps are stated in Fig. 5. The level of the final produce (B$_2$–SiNT (7, 0)–* + 2H$_2$O) is considered as reference step and ORR steps in $U = 0$ V is downhill. Reaction steps become downward that U is decreased to 0.97 V and beginning voltage for ORR is 0.97 V. The B$_2$–SiNT (7, 0) is suggested as suitable ORR catalyst.

4. Conclusions

Performances of boron–silicon nanotube (7, 0) as novel catalyst to ORR are investigated. The ORR on surface of B$_2$–SiNT can be continued through LH and ER mechanisms. The rate-determining stage ($\Delta E_a = 0.35$ eV) for ORR on B$_2$–SiNT (7, 0) surface is creation of B$_2$–SiNT (7, 0)–*OH structure. The calculated beginning voltage to ORR on surface of the B$_2$–SiNT (7, 0) is 0.37 V. In the acidic solution the beginning voltage to oxygen reduction process can be evaluated to 0.97 V. Results indicated that the B$_2$–SiNT (7, 0) is suggested as catalyst to ORR with suitable efficiency.

Conflicts of interest

There are no conflicts to declare.

References

1 H. A. Gasteiger and N. M. Marković, *Science*, 2009, **324**, 48.
2 J. B. Lee and Y. K. Park, *J. Power Sources*, 2006, **158**, 1251.
3 N. M. Marković, T. Schmidt, J. Stamenkovic and V. Ross, *Fuel Cells*, 2001, **1**, 105.
4 Z. W. Liu, F. Peng, H. J. Wang and H. Yu, *Catal. Commun.*, 2012, **29**, 11.
5 N. S. Lewis and D. G. Nocera, *Proc. Natl. Acad. Sci. U. S. A.*, 2006, **103**, 15729.
6 P. H. Matter and L. Zhang, *J. Catal.*, 2006, **239**, 83.
7 M. Winter, *Chem. Rev.*, 2004, **104**, 4245.
8 V. I. Zaikovskii, *J. Phys. Chem. B*, 2006, **110**, 6881.
9 W. Song and E. J. M. Hensen, *ACS Catal.*, 2014, **4**, 1885.
10 J. Liu, *ACS Catal.*, 2016, **7**, 34.
11 Y. Nie, L. Li and Z. D. Wei, *Chem. Soc. Rev.*, 2015, **44**, 2168.
12 M. E. Scofield, H. Q. Liu and S. S. Wong, *Chem. Soc. Rev.*, 2015, **44**, 5836.
13 M. Zhou, H. L. Wang and S. Guo, *Chem. Soc. Rev.*, 2016, **45**, 1273.
14 S. B. Yang, L. J. Zhi, K. Tang, X. L. Feng and J. Maier, *Adv. Funct. Mater.*, 2012, **22**, 3634.

15 R. Li, Z. D. Wei, X. L. Gou and W. Xu, *RSC Adv.*, 2013, **3**, 9978.

16 K. Gong, P. Du, F. Xia and Z. H. Durstock, *Science*, 2009, **323**, 760.

17 M. Li, L. Zhang, Q. Xu, J. Niu and Z. J. Xia, *J. Catal.*, 2014, **314**, 66.

18 A. Wang, B. Lin and H. Zhang, *Catal. Sci. Technol.*, 2017, **7**, 2362.

19 I. A. Pasti, N. M. Gavrilov and A. S. Dobrota, *Electrocatalysis*, 2015, **6**, 498.

20 X. J. Bo and L. P. Guo, *Phys. Chem. Chem. Phys.*, 2013, **15**, 2459.

21 B. Delley, *J. Chem. Phys.*, 2000, **113**, 7756.

22 J. P. Perdew and K. Burke, *Phys. Rev. Lett.*, 1996, **77**, 3865.

23 A. A. Verma, S. A. Bates, T. Anggara and C. Paolucci, *J. Catal.*, 2014, **312**, 179.

24 S. Ata, H. Yoon and C. Subramaniam, *Polymer*, 2014, **55**, 5276.

25 D. Janas and A. P. Herman, *Carbon*, 2014, **73**, 225.

26 C. C. Lawlor and C. M. Schauerman, *J. Mater. Chem. C*, 2015, **3**, 10256.

27 J. Alvarenga, P. R. Jarosz and C. M. Schauerman, *Appl. Phys. Lett.*, 2010, **97**, 19.

28 I. Rubinstein and E. Gileadi, *J. Electroanal. Chem.*, 2017, **108**, 191.

29 D. Banham and S. Ye, *J. Power Sources*, 2015, **285**, 334.

30 G. Wu, K. I. More and P. Xu, *Chem. Commun.*, 2013, **49**, 329.

31 S. Gong and Z. H. Zhu, *J. Appl. Phys.*, 2013, **114**, 74303.

32 K. Kordek and L. Jiang, *Adv. Energy Mater.*, 2018, **2018**, 1802936.

33 J. Liang, Y. Jiao, M. Jaroniec and S. Z. Qiao, *Angew. Chem., Int. Ed.*, 2012, **51**, 11496.

34 B. C. Han, *Phys. Rev. B: Condens. Matter Mater. Phys*, 2008, **77**, 075410.

35 K. Shinozaki, J. W. Zack, S. Pylypenko, B. S. Pivovar and S. S. Kocha, *Kinet. Catal.*, 2015, **54**, 255.

36 A. N. Valisi, *Electrocatalysis*, 2013, **3**, 108.

37 N. V. Smirnova, *J. Electrochem. Soc.*, 2013, **162**, 1.

38 H. A. Gasteiger, *Appl. Catal., B*, 2005, **56**, 9.

39 K. Qu, Y. Zheng, S. Dai and S. Z. Qiao, *Nanoscale*, 2015, **7**, 12598.

40 V. Datsyuk, M. Kalyva and K. Papagelis, *Carbon*, 2008, **46**, 833.

41 J. C. Li and Z. Q. Yang, *NPG Asia Mater.*, 2018, **10**, 461.

42 C. Zhu, S. Fu, J. Song, Q. Shi and D. Su, *Small*, 2017, **13**, 1603407.

43 C. Zhu, S. Fu, Q. Shi and D. Du, *Angew. Chem., Int. Ed.*, 2017, **56**, 13944.

44 B. Bayatsarmadi, Y. Zheng and A. Vasileff, *Small*, 2017, **13**, 1702002.

45 J. C. Li, S. Y. Zhao and P. X. Hou, *Nanoscale*, 2015, **7**, 19201.

46 N. S. Parimi, Y. Umasankar and P. Atanassov, *ACS Catal.*, 2012, **2**, 38.

47 F. Jaouen, *Electrochim. Acta*, 2007, **52**, 5975.

48 Y. Chu, L. Gu, X. Ju and H. Du, *Catalysts*, 2018, **8**, 245.

49 L. Wang and H. Dong, *J. Phys. Chem. C*, 2016, **1203**, 117427.

50 P. Zhang and B. Xiao, *Sci. Rep.*, 2014, **4**, 3821.

51 L. Zhang and Z. Xia, *J. Phys. Chem. C*, 2011, **115**, 11170.

52 P. Zhang and J. S. Lian, *Phys. Chem. Chem. Phys.*, 2012, **14**, 11715.

53 J. D. Wiggins-Camacho and K. J. Stevenson, *J. Phys. Chem. C*, 2011, **115**, 20002.

54 D. Xiong and X. Li, *Catalysts*, 2018, **8**, 301.

55 X. Hu and C. Liu, *New J. Chem.*, 2011, **35**, 2601.

56 Q. Wei and X. Tong, *Catalysts*, 2015, **5**, 1574.

57 Y. Zhao and L. Yang, *J. Am. Chem. Soc.*, 2013, **135**, 1201.

58 L. Ferrighi and M. Datteo, *J. Phys. Chem. C*, 2014, **118**, 223.

59 A. Bruix, K. M. Neyman and F. Illas, *J. Phys. Chem. C*, 2010, **114**, 14202.

60 J. Cai, *Nature*, 2010, **466**, 470.

61 T. Wassmann, A. P. Seitsonen and A. M. Saitta, *Phys. Rev. Lett.*, 2008, **101**, 096402.

62 Y. H. Lu, R. Q. Wu, L. Shen, M. Yang and Z. D. Sha, *Appl. Phys. Lett.*, 2009, **94**, 122111.

63 R. S. Mulliken, *J. Chem. Phys.*, 1955, **23**, 18330.

64 N. Govind, *Comput. Mater. Sci.*, 2003, **28**, 250.

65 C. T. Campbell and J. R. V. Sellers, *Faraday Discuss.*, 2013, **162**, 9.

66 J. K. Nørskov and J. Rossmeisl, *J. Phys. Chem. B*, 2004, **108**, 17886.

67 S. Royer and D. Duprez, *ChemCatChem*, 2011, **3**, 24.

68 M. S. Chen, Y. Cai and Z. Yan, *Surf. Sci.*, 2007, **601**, 5326.

69 M. A. Yu, Y. Feng, L. Gao and S. Lin, *Phys. Chem. Chem. Phys.*, 2018, **20**, 20661.

70 J. A. Keith and T. Jacob, *Angew. Chem., Int. Ed.*, 2010, **49**, 9521.

71 Y. Sha, T. H. Yu, Y. Liu and B. V. Merinov, *J. Phys. Chem. Lett.*, 2010, **1**, 856.

72 X. W. Yu and S. Y. Ye, *J. Power Sources*, 2007, **172**, 145.

73 A. J. Cohen, P. Mori-Sánchez and W. Yang, *Chem. Rev.*, 2012, **112**, 289.

74 E. Skulason, *Phys. Chem. Chem. Phys.*, 2007, **9**, 3241.

75 Y. X. Chen, *Angew. Chem., Int. Ed.*, 2012, **51**, 8500.

76 W. Y. Zhang, *Electrochim. Acta*, 2016, **200**, 131.

77 H. Jeon, *J. Power Sources*, 2010, **195**, 5929.

78 J. Shui, *Sci. Adv.*, 2015, **1**, 1.

79 C. Bianchini, *Chem. Rev.*, 2009, **109**, 4183.

80 E. DeCarlos and J. G. Ángyán, *J. Chem. Phys.*, 2016, **145**, 124105.

81 P. Kasper, *J. Phys. Chem. A*, 2017, **121**, 2022.

82 G. Michael and I. S. Bushmarinov, *Science*, 2017, **355**, 49.

83 M. Nielsen, *Surf. Sci.*, 2015, **631**, 2.

84 M. H. Shao, *J. Power Sources*, 2011, **196**, 2433.

85 D. H. Guo, *Science*, 2016, **351**, 361.

86 S. E. Wheeler, A. Moran, S. N. Pieniazek and K. N. Houk, *J. Phys. Chem. A*, 2009, **113**, 10376.

87 J. Hohenstein, *Chem. Phys.*, 2006, **15**, 128.

88 G. Fazio, L. Ferrighi and C. Di Valentin, *J. Catal.*, 2014, **318**, 203.

89 V. Tripkovic and E. Skulason, *Electrochim. Acta*, 2010, **55**, 7975.

90 M. J. Janik, C. D. Taylor and M. Neurock, *J. Electrochem. Soc.*, 2009, **156**, 126.

91 J. X. Zhao, C. R. Cabrera, Z. H. Xia and Z. F. Chen, *Carbon*, 2016, **104**, 56.

92 L. H. Gan and J. Q. Zhao, *Phys. E*, 2009, **41**, 1249.

93 S. F. Boys and F. Bernardi, *Mol. Phys.*, 1970, **19**, 553.

94 L. Ma, J. M. Zhang, K. W. Xu and V. Ji, *Appl. Surf. Sci.*, 2015, **343**, 121.

95 B. Luo, *Small*, 2012, **8**, 630.

96 J. B. Zhu, *J. Mater. Chem. A*, 2016, **4**, 7422.

97 G. Kresse and M. Hafner, *Phys. Rev. B: Condens. Matter Mater. Phys*, 1993, **47**, 558.

98 X. K. Kong, *Chem. Soc. Rev.*, 2014, **43**, 2841.

99 J. C. Liu, Y. G. Wang and J. Li, *J. Am. Chem. Soc.*, 2017, **139**, 6190.

100 Z. Qi, *J. Power Sources*, 2011, **196**, 5823.

101 M. Branda, N. C. Hernández, J. F. Sanz and F. Illas, *J. Phys. Chem. C*, 2010, **114**, 1934.

102 G. Henkelman, B. P. Uberuaga and H. Jónsson, *J. Chem. Phys.*, 2000, **113**, 9901.

103 A. J. Binder, T. J. Toops and R. R. Unocic, *Angew. Chem., Int. Ed.*, 2015, **54**, 13263.

104 E. Y. Ko, E. D. Park, H. C. Lee and D. Lee, *Angew. Chem., Int. Ed.*, 2007, **46**, 734.

105 S. Zhao, H. Zhang, S. D. House, R. Jin and R. Jin, *ChemElectroChem*, 2016, **3**, 1225.

106 G. Ramos-Sánchez and H. Yee-Madeira, *Int. J. Hydrogen Energy*, 2008, **33**, 3596.

107 M. Neergat, V. Gunasekar and R. Rahul, *J. Electroanal. Chem.*, 2011, **658**, 25.

108 Y. Dai, P. Yu, Q. Huang and K. Sun, *Fuel Cells*, 2016, **16**, 165.

109 L. Xiong, Y. X. Huang, X. W. Liu and W. W. Li, *Electrochim. Acta*, 2013, **89**, 24.

110 W. E. Mustain, K. Kepler and M. Prakash, *Electrochem. Commun.*, 2006, **8**, 406.